


Invited Article: Precision nanoimplantation of nitrogen vacancy centers into diamond photonic crystal cavities and waveguides

Cite as: APL Photonics 1, 020801 (2016); <https://doi.org/10.1063/1.4948746>

Submitted: 26 February 2016 . Accepted: 26 April 2016 . Published Online: 23 May 2016

M. Schukraft , J. Zheng, T. Schröder , S. L. Mouradian, M. Walsh, M. E. Trusheim, H. Bakhru, and D. R. Englund

COLLECTIONS

 This paper was selected as Featured



View Online



Export Citation



CrossMark

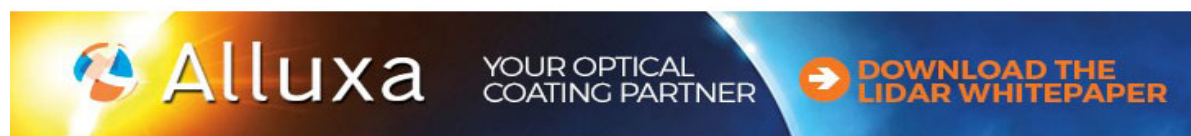
ARTICLES YOU MAY BE INTERESTED IN

[Invited Article: Broadband highly efficient dielectric metadevices for polarization control](#)
APL Photonics 1, 030801 (2016); <https://doi.org/10.1063/1.4949007>

[A tunable waveguide-coupled cavity design for scalable interfaces to solid-state quantum emitters](#)

APL Photonics 2, 046103 (2017); <https://doi.org/10.1063/1.4978204>

[Why I am optimistic about the silicon-photonics route to quantum computing](#)
APL Photonics 2, 030901 (2017); <https://doi.org/10.1063/1.4976737>



Invited Article: Precision nanoimplantation of nitrogen vacancy centers into diamond photonic crystal cavities and waveguides

M. Schukraft,^{1,2,a,b} J. Zheng,^{1,3,a} T. Schröder,¹ S. L. Mouradian,¹ M. Walsh,¹ M. E. Trusheim,¹ H. Bakhru,⁴ and D. R. Englund^{1,c}

¹*Department of Electrical Engineering and Computer Science, Massachusetts Institute of Technology, Cambridge, Massachusetts 02139, USA*

²*School of Basic Sciences, Ecole Polytechnique Fédérale de Lausanne, Lausanne, Vaud 1015, Switzerland*

³*Department of Electrical Engineering, Columbia University, New York, New York 10027, USA*

⁴*SUNY Polytechnic Institute Colleges of Nanoscale Science and Engineering, Albany, New York 12203, USA*

(Received 26 February 2016; accepted 26 April 2016; published online 23 May 2016)

We demonstrate a self-aligned lithographic technique for precision generation of nitrogen vacancy (NV) centers within photonic nanostructures on bulk diamond substrates. The process relies on a lithographic mask with nanoscale implantation apertures for NV creation, together with larger features for producing waveguides and photonic nanocavities. This mask allows targeted nitrogen ion implantation, and precision dry etching of nanostructures on bulk diamond. We demonstrate high-yield generation of single NVs at pre-determined nanoscale target regions on suspended diamond waveguides. We report implantation into the mode maximum of diamond photonic crystal nanocavities with a single-NV per cavity yield of ~26% and Purcell induced intensity enhancement of the zero-phonon line. The generation of NV centers aligned with diamond photonic structures marks an important tool for scalable production of optically coupled spin memories. © 2016 Author(s). All article content, except where otherwise noted, is licensed under a Creative Commons Attribution (CC BY) license (<http://creativecommons.org/licenses/by/4.0/>). [<http://dx.doi.org/10.1063/1.4948746>]

A key challenge for quantum information science is to efficiently entangle multiple quantum memories for quantum networking and distributed quantum computing. The negatively charged nitrogen vacancy (NV) defect center in diamond satisfies critical requirements for solid-state qubits^{1,2} and stands out as one of the most promising atom-like solid state defects due to its optical addressability and long-lived electronic and nuclear spin states.³ Electron spin coherence times have been observed to be in the milliseconds regime at room temperature⁴ and approaching one second at cryogenic temperatures.⁵ These properties have enabled demonstrations of NV based quantum registers,⁶ qubit gates,⁷ and NV-photon entanglement.⁸ Recently, NV-to-NV quantum entanglement⁹ and teleportation¹⁰ have been shown, conceivably enabling a network of numerous NVs remotely entangled via two-photon quantum interference.¹¹

However, the generation of scalable quantum networks is currently hindered by a slow entanglement rate (1 event per ~250 s¹⁰) compared to the NV spin decoherence rate. Photon-mediated entanglement relies on the successful entanglement of NV-emitted photons with its electron spin.¹² Only photons emitted via the NV zero-phonon line (ZPL) can exhibit this property.¹³ However, the NV natural decay rate into the ZPL is small, determined by a Debye Waller (DW) factor of ~3%;¹⁴

^aM. Schukraft and J. Zheng contributed equally to this work.

^bElectronic mail: mschuk@mit.edu

^c<http://www.rle.mit.edu/qp/>

additionally, spatial collection and transmission losses limit the entanglement rate. An established approach to increase spontaneous emission rates is to couple NVs to photonic cavities.^{15,16} When an NV is located in a cavity with quality factor Q and mode volume $V_{\text{mode}} \sim (\lambda/n)^3$, the spectrally resolved spontaneous emission rate via its 637 nm ZPL is enhanced by the Purcell factor

$$F_{\text{ZPL}} = \xi F_{\text{ZPL}}^{\text{max}} \frac{1}{1 + 4Q^2(\lambda_{\text{ZPL}}/\lambda_{\text{cav}} - 1)^2}, \quad (1)$$

where $F_{\text{ZPL}}^{\text{max}} = \frac{3}{4\pi^2} \left(\frac{\lambda_{\text{cav}}}{n} \right)^3 \frac{Q}{V_{\text{mode}}}$ is the maximum spontaneous emission (SE) rate enhancement and $\xi = \left(\frac{|\vec{\mu}(\vec{r}) \cdot \vec{E}(\vec{r})|}{|\vec{\mu}(\vec{r})| |\vec{E}_{\text{max}}(\vec{r})|} \right)^2$ quantifies the angular and spatial overlap between the dipole moment ($\vec{\mu}$) of the NV ZPL transition and the cavity mode electric field (\vec{E}).¹⁷ The rate of entanglement between two separated NVs scales approximately with β^2/DW^2 in the regime of long distances,⁸ where $\beta = \frac{F_{\text{ZPL}} DW}{1 + F_{\text{ZPL}} DW}$ is the probability that the NV emits via the cavity mode to a single-mode optical link.¹⁷ Therefore, large improvements in entanglement rates can be achieved via NV-cavity coupling for F_{ZPL} approaching $\frac{1}{DW} \sim 30 - 40$. Recently NV-cavity systems were fabricated with Purcell enhancement up to $F_{\text{ZPL}} \sim 60$ (at cryogenic temperatures),^{18,19} in principle allowing for a $\sim 10^3$ speed-up of the entanglement rate simply by redistributing emission into the ZPL and increasing its transition rates,¹⁸ further enhancements are possible with improved spatial collection efficiency from the nanocavity.

To reach high Purcell enhancement, cavities are typically designed²⁰ with small mode volumes V_{mode} . However, small mode volumes also require precise and accurate NV spatial positioning into the mode maximum to reach near-unity overlap ξ . For the diamond cavity type discussed in this paper, the NV must be placed within a $100 \times 20 \times 40 \text{ nm}^3$ volume (within 90% of the mode intensity maximum, represented in Fig. 2(b)) to achieve at least 90% of the maximum achievable Purcell enhancement $F_{\text{ZPL}}^{\text{max}}$. Traditional techniques for NV creation^{21,22} lack scalability. Targeted NV creation can be achieved by focused nitrogen (N) ion beam implantation,²³ or implantation through nano-apertures defined in an e-beam resist layer^{24,25} but precise alignment is challenging as it involves a two-step lithography process with mask overlay (masks for patterning and implantation are separate). Existing techniques that allow more precise NV-cavity alignment, such as ion implantation through a pierced atomic-force microscope (AFM) tip,²⁶ rely on a time-consuming serial alignment and implantation process.

In this work we demonstrate a recently introduced nanofabrication method on bulk diamond^{27,28} that allows tens of nanometers precision in NV-to-cavity alignment while maintaining high parallel fabrication throughput. Our technique makes use of a single silicon (Si) hard mask for both patterning (by reactive ion etching of diamond) and generation of NV centers (by N implantation and subsequent annealing). Because the same mask is used for the N implantation and diamond patterning, we are no longer limited by the alignment accuracy of a two-step lithography process; instead we are limited by the aperture size and the implantation straggle. Limitations due to aperture size can be overcome by narrowing the aperture down to $\sim 1 \text{ nm}$ via atomic layer deposition,²⁹ and limitations due to the ion scattering by the aperture sidewalls can be minimized by precise sample stage tilt control ($\pm 0.1^\circ$ in our process) for perpendicular positioning of the diamond surface with respect to the ion beam. The remaining limitation is the implantation straggle of $\sim 20 \text{ nm}$ for a $\sim 100 \text{ keV}$ implantation beam according to SRIM simulations.³⁰ We demonstrate that our self-aligned lithography technique makes it possible to produce NV-cavity systems with consistently high success probability. We also show high-yield creation of single NVs in waveguide-integrated photonic cavities and report successful NV-cavity coupling with Purcell induced intensity enhancement of the NV ZPL emission.

We created one dimensional waveguide-integrated photonic NV-cavity systems (Fig. 1) fabricated in a monolithic all-diamond approach for maximum NV dipole to cavity mode overlap.³¹ The cavity³² consists of a suspended 1D diamond photonic crystal (PhC) structure with triangular cross section, with lattice constant a , hole parameters $W_X = 0.61a$ and $W_Z = 0.32a$, beam width $W = 3.82a = 450 \text{ nm}$, and beam thickness $h = 1.1a$. The defect state is defined by a linear lattice increase from $0.9a$ in the cavity center to a with constant increment of $0.02a$. To reach a high $F_{\text{ZPL}}^{\text{max}}$,

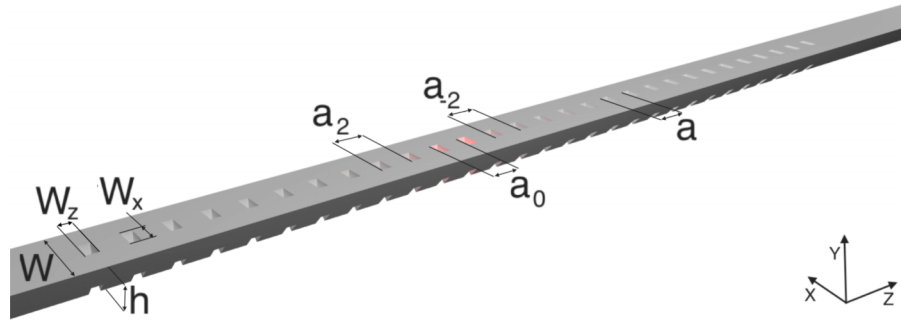


FIG. 1. Schematics of the intended NV-cavity system. Perspective view of the all-diamond photonic waveguide of triangular cross section, of beam width W and beam thickness h , and its integrated one dimensional photonic cavity, of lattice constant a and hole parameters W_x and W_z .

cavity parameters were optimized³² to obtain a low mode volume V_{mode} and for the fundamental cavity resonance λ_{cav} to overlap with the NV ZPL emission wavelength $\lambda_{\text{ZPL}} = 637$ nm.

We integrated these NV-cavity systems into photonic waveguides to provide collection capability for NV photons into a single spatial mode, also enabling collection of photons coherent with the NV state for entanglement mediation.¹⁵ One-sided cavity-waveguide coupling was achieved by a discontinuity of the PhC on one side of the cavity after 10 periods (while it extends on the opposite side for 17 periods). Finite difference time domain (FDTD, Lumerical) simulations estimate unloaded Q values of $\sim 30\,000$ and predict waveguide-loaded Q values of ~ 500 -800 with intended cavity loss primarily into the single waveguide mode. We aimed to create a single NV, ideally at the mode maximum of the cavity (Fig. 2), to couple with the cavity mode.

The sample was fabricated on a $2 \times 2 \times 0.5$ mm³ electronic grade (N impurity below 5 ppb) single-crystal bulk diamond chip (commercially available, Element Six) grown by microwave plasma enhanced chemical vapor deposition (MPECVD). We used the same 1×1 mm² sized mask for both N ion implantation and reactive ion etching. The mask patterns (waveguides, PhC cavities, and implantation apertures) were defined in the same e-beam exposure on a 270 nm silicon-on-insulator wafer (SOITEC) and transferred into the Si layer via a mixture of sulfur hexafluoride and oxygen reactive ion etching (RIE).³³ This Si hard mask is shown in Fig. 3(a). In addition to the photonic devices (Fig. 3(a), top), the mask also contains narrow rectangular holes of less than 50 nm width (Fig. 3(a) inset bottom left) which we refer to as implantation apertures. Their small width and high aspect ratio ($270:40 = 6.75$, where 270 nm is the thickness of the Si hard mask, and 40 nm is the width of the implantation aperture as shown in Fig. 3(a) in the lower left

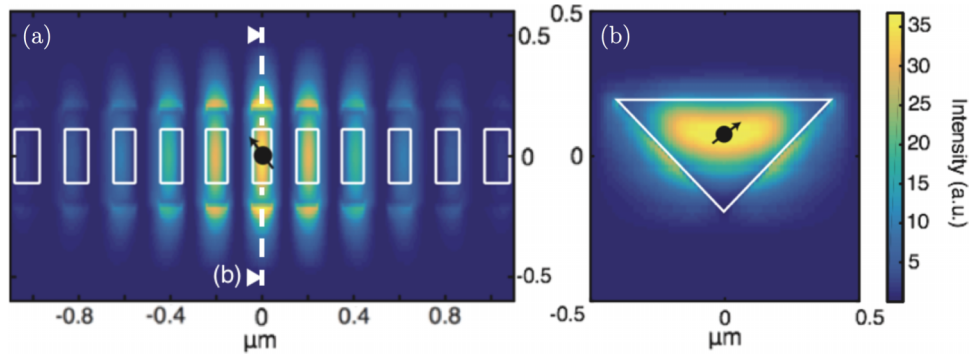


FIG. 2. Cavity field simulations. Map of the electric field intensity of the fundamental cavity mode in (a) plane ($y = 0.55a$) and (b) cross section ($z = 0$). The white lines delineate the diamond, while the yellow areas (mode intensity values above 90% of the mode intensity maximum, i.e., above ~ 32 a.u.) represent the $100 \times 20 \times 40$ nm³ volume in which the NV has to be created to reach 90% spatial overlap with the cavity field. The NV defect, with dipolar moment $\vec{\mu}$, is here ideally represented at the cavity mode maximum.

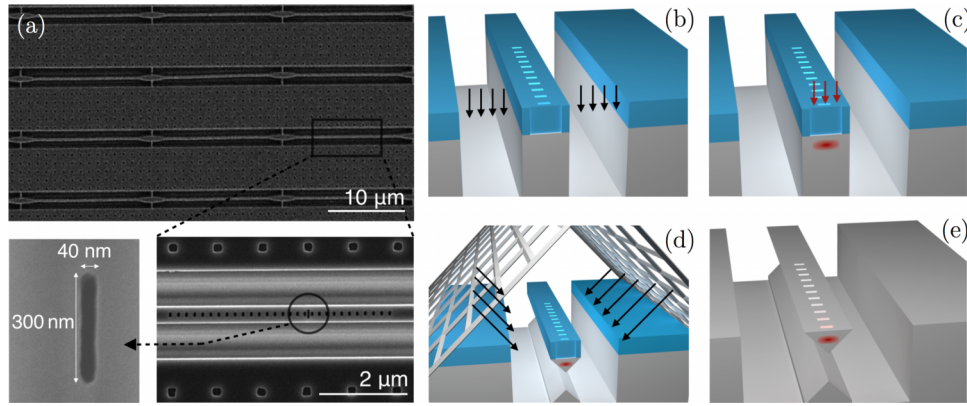


FIG. 3. Scanning electron micrograph (SEM) of Si mask and fabrication scheme. (a) Si mask for the production of arrays of waveguide-integrated NV-cavity systems. The bottom right inset shows an exemplary waveguide-integrated 1D photonic cavity pattern, with the implantation aperture centered at its mode maximum (in this device the PhC holes were slightly underdeveloped). The bottom left inset zooms into an implantation aperture. (b) Photonic pattern transfer into diamond via vertical plasma etching. (c) Implantation of ^{15}N ions. (d) Free-standing waveguide structures achieved via angular plasma etching.³⁷ (e) Resulting structure after Si mask removal and annealing. The red colored glow represents NV emission.

panel) prevent oxygen ion etching through them due to RIE lag.³⁴ The transport of oxygen reactant and etching byproduct is significantly attenuated along the high aspect ratio implantation aperture,^{35,36} leading to a negligible etching rate for the diamond surface in the aperture. On the other hand, N ions from the implanter can easily pass through the aperture and implant into the diamond, because the ion energy (100 keV) and chamber pressure (0.3 μTorr) are orders of magnitude larger and smaller, respectively, than during plasma etching (10 mTorr, ~ 40 V bias voltage). The photonic features in the mask are relatively low in aspect ratio and are transferred during oxygen RIE into the diamond as waveguides and PhC cavities.³⁶ The rectangular implantation apertures are aligned with the waveguide and cavity patterns, restricting the implantation volume solely to the predefined mode maxima (Fig. 3(a) inset bottom right). Additional fabrication details were described in our previous work.³²

We released the Si mask membrane from the SOI chip in 49% hydrofluoric acid and transferred it onto the diamond.^{18,33} The sample was then dry etched using an O_2 plasma to a depth of ~ 1.6 μm (Fig. 3(b)). Subsequently we implanted ^{15}N ions with an ion energy of 100 keV (predicted mean penetration depth of 110 nm,³⁰ chosen to match the depth of the cavity mode maximum) at a dosage of 10^{11} N/cm² (Fig. 3(c)). Using a $\sim 45^\circ$ angled O_2 plasma etching via the use of a Faraday cage (Fig. 3(d))³⁷ we undercut the photonic crystal structures to create free-standing waveguides of triangular cross section. We removed the Si mask (Fig. 3(e)) by placing the sample in a hot KOH solution. Finally, we annealed the diamond at 850° for two hours in an oxygen enriched atmosphere to form NVs,³⁸ for which we expect an N-to-NV conversion efficiency of ~ 1 -10%.^{39,40}

Our fabrication process enables parallel fabrication of thousands of waveguides and PhC cavities (Fig. 4) with NVs at their mode maximum. Due to the stochastic nature⁴¹ of the implantation and the N-to-NV conversion, the number of created NVs follows a Poissonian probability distribution $f_p(\lambda)$, where λ is the event rate. Implantation dose and aperture size were selected to create a single NV per cavity on average; therefore, we expect a Poisson distribution with parameters approaching $\text{Var}(N_{\text{NV}}) = \langle N_{\text{NV}} \rangle = 1$ and a corresponding single NV-cavity system yield close to $f_p(\lambda = 1) = e^{-1} \sim 37\%$.

We first characterized the samples by room-temperature photoluminescence (PL) scans using a scanning confocal microscope with 532 nm continuous-wave laser excitation. The PL was collected into an optical fiber connected either to an avalanche photodiode or a spectrometer. Fig. 5(a) shows a typical PL scan of an array of waveguides. With higher resolution PL scans around cavity centers, as in Fig. 5(b), we identified local increases in fluorescence which indicate the potential presence of an NV center. We verified NV centers by their unique fluorescence spectra with ZPL emission at 637 nm and a broad phonon side band, as shown in Fig. 5(c).

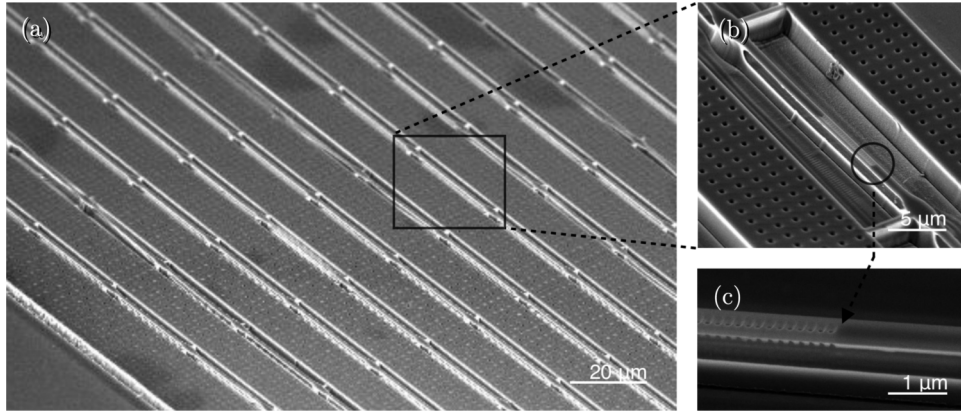


FIG. 4. Fabricated diamond nanostructures. (a) Arrays of waveguides. (b) Representative free-standing waveguide with an integrated waveguide-loaded photonic cavity. (c) Higher resolution image revealing the triangular cross section.

To quantify the number of NVs created in a given spot, we measured the photon emission statistics using a Hanbury Brown Twiss (HBT) setup⁴² and normalized the resulting second-order auto-correlation measurements $g^{(2)}(\tau)$. We measured both the photon count rates at the NV position and the background fluorescence to correct for the presence of uncorrelated background photon emission.^{43,44} By fitting the zero-delay dip in the $g^{(2)}(\tau)$ function, we evaluated the number of emitting NV defects created per cavity. The anti-bunching dip in the $g^{(2)}(\tau)$ function, observed at zero time delay $\tau = 0$, is the signature of a single photon emitter for $g^{(2)}(0) < 0.5$ (Fig. 6(a), bottom) or of n multiple single photon emitters of equal intensity for $1 - \frac{1}{n+1} > g^{(2)}(0) > 1 - \frac{1}{n}$ (Fig. 6(a), top).³

By repeating these measurements across the chip, we evaluated the number of cavities in which a single NV was created, i.e., the NV-cavity yield we achieved. The histogram in Fig. 6(b) summarizes results sampled over 45 cavity centers. We observed a mean of $\langle N_{NV} \rangle = 0.44$ NV centers per spot with a variance of 0.51. The histogram is closely fit by a Poissonian probability distribution, as expected, with a mean and variance of 0.39. We estimate a single NV-cavity system yield of $26 \pm 1\%$ (Fig. 6(b), blue) confirming the scalability of this fabrication method (close to the 37% theoretical limit).

We investigated how well the NVs implanted through self-aligned apertures were coupled to the cavities. These experiments were performed at room temperature and show NV-cavity coupling. We focused the 532 nm laser at cavity centers and collected the emitted PL for spectral analysis to infer both the cavity resonance frequency and Q factor. We compared “empty” cavities with cavities

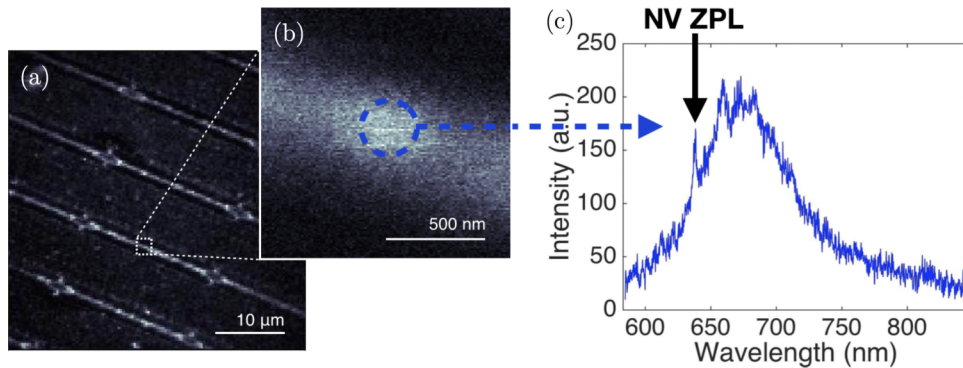


FIG. 5. Optical characterization. (a) Fluorescence scan of suspended diamond waveguides. (b) High resolution PL scan around a cavity center revealing a bright spot, identified as an NV center by PL spectral analysis (c) which featured a sharp ZPL and broad phonon side band which are characteristic of the NV emission spectrum. At this particular cavity center, we saw only the NV spectrum as no resonance was present.

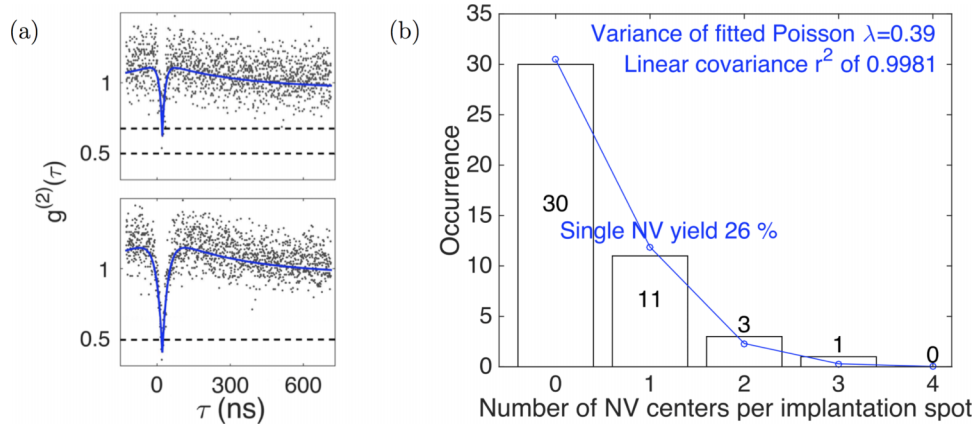


FIG. 6. Single NV implantation statistics. (a) Normalized second-order auto-correlation function measurements of a single and a double NV centre. In the bottom plot, $g^{(2)}(0) \sim 0.4$ indicates that the fluorescence originates from a single NV center (dotted line, $g^{(2)}(0) < 0.5$), while the upper plot reads $g^{(2)}(0) \sim 0.6$ indicating the presence of a double NV center (dotted lines, $0.5 < g^{(2)}(0) < 0.67$). Performing this discriminating experiment at 45 cavity centers we determined statistics about the single NV creation efficiency. (b) Distribution of the number of NV defects per cavity evaluated on 45 sites, fitted to a Poisson distribution.

that contained NVs. The PL spectrum of an empty cavity (Fig. 7(a)) reveals a cavity resonance close to the targeted ZPL emission wavelength $\lambda_{\text{ZPL}} = 637$ nm, and a waveguide-loaded Q factor of ~ 260 .

For cavities in which a single NV was created, we observed spectral overlap between the broadband fluorescence of the NV and the resonant frequency of the cavity which demonstrates coupling

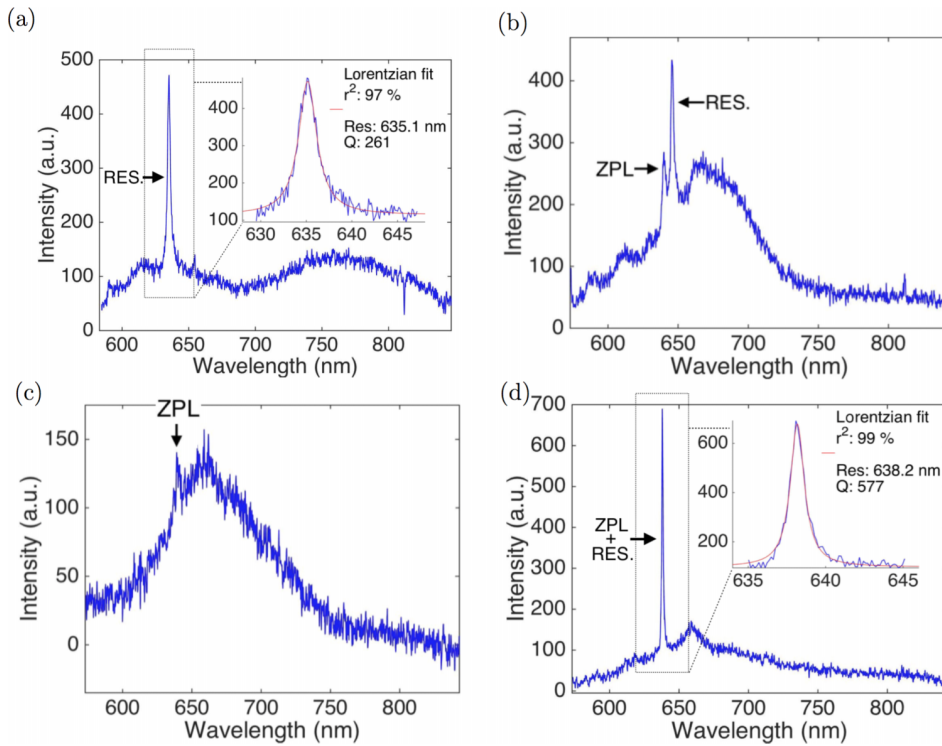


FIG. 7. NV-cavity coupling characterization. (a) Measured fundamental cavity resonance in an NV deprived cavity. The inset displays a Lorentzian fit estimating a corresponding Q factor of 261 and a resonance at 635 nm. (b) Spectral measurement of an NV-cavity system rendering ZPL and cavity resonance both evident and detuned by only 2 nm. (c) Spectrum of an NV-cavity system with suppressed resonance displaying a characteristic NV spectrum. Both ZPL and the accumulated phonon sidebands are apparent. (d) Same system as in (c) with the polarizer tuned to maximize the cavity resonance. A Lorentzian fit plotted in the inset yields a Q factor of 577 at a resonance of 638 nm.

of the implanted NV to a cavity mode. Fig. 7(b) shows the spectrum of such an NV-cavity system, with the NV typical spectral features, with an overlapping cavity resonance detuned from the ZPL by a few nm. However, as mentioned, integration of NV-cavity centers for quantum entanglement applications requires $\lambda_{\text{cav}} \approx \lambda_{\text{ZPL}}$ to reach significant Purcell enhancement F_{ZPL} . For one NV-cavity system, nearly exact spectral overlap of the resonance with the ZPL was observed. Fig. 7(c) plots its PL spectrum with a polarizer mounted in front of the spectrometer, filtering out the cavity resonance, and only transmitting NV fluorescence that is not modified by the cavity mode, revealing a characteristic NV spectrum. In Fig. 7(d) the same system is plotted, but with the polarizer maximizing the cavity resonance, thus revealing the fluorescence from both the ZPL directly and scattered through the cavity mode. We estimated the corresponding intensity enhancement to be ~ 4.9 via the ratio of cross-polarized intensities.

The demonstrated Purcell induced intensity enhancement is comparable to cavity induced NV ZPL intensity values previously reported for waveguide-coupled NV-cavity systems.^{31,45,46} Although such enhancements are lower than those demonstrated for non-waveguide-coupled NV-cavity systems,^{18,19} we emphasize that waveguide coupling is a requirement for entanglement mediation of on-chip networks where waveguides provide photonic routing. Nevertheless, through fabrication improvements and waveguide-coupling optimization, larger enhancement factors can be expected. While waveguide coupling allows guided photon transfer for entanglement schemes, it also reduces Q values and therefore further work could be directed towards the realization of waveguide-integrated cavities where this trade-off is optimized for overall entanglement probability between two waveguide-connected NV-cavity systems.

In summary, we have demonstrated a fabrication technique based on self-aligned ion implantation via a combined etching and implantation mask that allows tens of nanometers precision in NV-to-cavity alignment while maintaining high parallel fabrication throughput. This process allows targeted creation of single NV centers in complex photonic nanostructures, in particular at the mode maximum of cavities embedded in arrays of photonic waveguides. We demonstrated that this method enables the fabrication of NV-cavity systems with a yield of $\sim 26\%$ and verified NV-cavity coupling with a ~ 5 -fold Purcell induced intensity enhancement of the NV ZPL emission.

Our work establishes that NV-nanocavity systems can be fabricated effectively by self-aligned positioning of NVs into the cavity field maximum. Because of the great simplicity of implanting and fabricating with the same mask, we expect that this process will accelerate work towards extended on-chip photonic networks that could rapidly produce entanglement across multiple NV-cavity systems for quantum networking and distributed quantum computing.

Fabrication and experiments were supported in part by the Air Force Office of Scientific Research PECASE (supervised by Gernot Pomrenke), the AFOSR Quantum Memories MURI, and the U.S. Army Research Laboratory (ARL) Center for Distributed Quantum Information (CDQI). Research carried out in part at the Center for Functional Nanomaterials, Brookhaven National Laboratory, which is supported by the U.S. Department of Energy, Office of Basic Energy Sciences, under Contract No. DE-SC0012704. M.S. was supported in part also by the Hasler Stiftung. T.S. was supported in part by the ARL CDQI. J.Z. would like to thank Ming Lu and Aaron Stein for their advice and assistance.

¹ M. G. Dutt, L. Childress, L. Jiang, E. Togan, J. Maze, F. Jelezko, A. Zibrov, P. Hemmer, and M. Lukin, "Quantum register based on individual electronic and nuclear spin qubits in diamond," *Science* **316**, 1312–1316 (2007).

² P. Neumann, N. Mizuochi, F. Rempp, P. Hemmer, H. Watanabe, S. Yamasaki, V. Jacques, T. Gaebel, F. Jelezko, and J. Wrachtrup, "Multipartite entanglement among single spins in diamond," *Science* **320**, 1326–1329 (2008).

³ M. W. Doherty, N. B. Manson, P. Delaney, F. Jelezko, J. Wrachtrup, and L. C. Hollenberg, "The nitrogen-vacancy colour centre in diamond," *Phys. Rep.* **528**, 1–45 (2013).

⁴ G. Balasubramanian, P. Neumann, D. Twitchen, M. Markham, R. Kolesov, N. Mizuochi, J. Isoya, J. Achard, J. Beck, J. Tissler *et al.*, "Ultralong spin coherence time in isotopically engineered diamond," *Nat. Mater.* **8**, 383–387 (2009).

⁵ N. Bar-Gill, L. M. Pham, A. Jarmola, D. Budker, and R. L. Walsworth, "Solid-state electronic spin coherence time approaching one second," *Nat. Commun.* **4**, 1743 (2013).

⁶ P. Neumann, N. Mizuochi, F. Rempp, P. Hemmer, H. Watanabe, S. Yamasaki, V. Jacques, T. Gaebel, F. Jelezko, and J. Wrachtrup, "Multipartite entanglement among single spins in diamond," *Science* **320**, 1326–1329 (2008).

⁷ T. Gaebel, M. Domhan, I. Popa, C. Wittmann, P. Neumann, F. Jelezko, J. R. Rabeau, N. Stavrias, A. D. Greentree, S. Prawer *et al.*, "Room-temperature coherent coupling of single spins in diamond," *Nat. Phys.* **2**, 408–413 (2006).

- ⁸ E. Togan, Y. Chu, A. Trifonov, L. Jiang, J. Maze, L. Childress, M. G. Dutt, A. S. Sørensen, P. Hemmer, A. Zibrov *et al.*, "Quantum entanglement between an optical photon and a solid-state spin qubit," *Nature* **466**, 730–734 (2010).
- ⁹ H. Bernien, B. Hensen, W. Pfaff, G. Koolstra, M. Blok, L. Robledo, T. Taminiau, M. Markham, D. Twitchen, L. Childress *et al.*, "Heralded entanglement between solid-state qubits separated by three metres," *Nature* **497**, 86–90 (2013).
- ¹⁰ W. Pfaff, B. Hensen, H. Bernien, S. B. van Dam, M. S. Blok, T. H. Taminiau, M. J. Tiggelman, R. N. Schouten, M. Markham, D. J. Twitchen *et al.*, "Unconditional quantum teleportation between distant solid-state quantum bits," *Science* **345**, 532–535 (2014).
- ¹¹ A. Sipahigil, M. L. Goldman, E. Togan, Y. Chu, M. Markham, D. J. Twitchen, A. S. Zibrov, A. Kubanek, and M. D. Lukin, "Quantum interference of single photons from remote nitrogen-vacancy centers in diamond," *Phys. Rev. Lett.* **108**, 143601 (2012).
- ¹² B. Hensen, H. Bernien, A. Dréau, A. Reiserer, N. Kalb, M. Blok, J. Ruitenbergh, R. Vermeulen, R. Schouten, C. Abellán *et al.*, "Loophole-free bell inequality violation using electron spins separated by 1.3 kilometres," *Nature* **526**, 682–686 (2015).
- ¹³ H. Bernien, L. Childress, L. Robledo, M. Markham, D. Twitchen, and R. Hanson, "Two-photon quantum interference from separate nitrogen vacancy centers in diamond," *Phys. Rev. Lett.* **108**, 043604 (2012).
- ¹⁴ H.-Q. Zhao, M. Fujiwara, and S. Takeuchi, "Suppression of fluorescence phonon sideband from nitrogen vacancy centers in diamond nanocrystals by substrate effect," *Opt. Express* **20**, 15628–15635 (2012).
- ¹⁵ H. J. Kimble, "The quantum internet," *Nature* **453**, 1023–1030 (2008).
- ¹⁶ S. Noda, M. Fujita, and T. Asano, "Spontaneous-emission control by photonic crystals and nanocavities," *Nat. Photonics* **1**, 449–458 (2007).
- ¹⁷ C. Santori, D. Fattal, and Y. Yamamoto, *Single-Photon Devices and Applications* (John Wiley & Sons, 2010).
- ¹⁸ L. Li, T. Schröder, E. H. Chen, M. Walsh, I. Bayn, J. Goldstein, O. Gaathon, M. E. Trusheim, M. Lu, J. Mower *et al.*, "Coherent spin control of a nanocavity-enhanced qubit in diamond," *Nat. Commun.* **6**, 6173 (2015).
- ¹⁹ A. Faraon, C. Santori, Z. Huang, V. M. Acosta, and R. G. Beausoleil, "Coupling of nitrogen-vacancy centers to photonic crystal cavities in monocrystalline diamond," *Phys. Rev. Lett.* **109**, 033604 (2012).
- ²⁰ T. Tiecke, J. D. Thompson, N. P. de Leon, L. Liu, V. Vuletić, and M. D. Lukin, "Nanophotonic quantum phase switch with a single atom," *Nature* **508**, 241–244 (2014).
- ²¹ J. Orwa, C. Santori, K. Fu, B. Gibson, D. Simpson, I. Aharonovich, A. Stacey, A. Cimmino, P. Balog, M. Markham *et al.*, "Engineering of nitrogen-vacancy color centers in high purity diamond by ion implantation and annealing," *J. Appl. Phys.* **109**, 083530 (2011).
- ²² J. C. Lee, D. O. Bracher, S. Cui, K. Ohno, C. A. McLellan, X. Zhang, P. Andrich, B. Alemán, K. J. Russell, A. P. Magyar *et al.*, "Deterministic coupling of delta-doped nitrogen vacancy centers to a nanobeam photonic crystal cavity," *Appl. Phys. Lett.* **105**, 261101 (2014).
- ²³ M. Lesik, P. Spinicelli, S. Pezzagna, P. Happel, V. Jacques, O. Salord, B. Rasser, A. Delobbe, P. Sudraud, A. Tallaire *et al.*, "Maskless and targeted creation of arrays of colour centres in diamond using focused ion beam technology," *Phys. Status Solidi A* **210**, 2055–2059 (2013).
- ²⁴ D. M. Toyli, C. D. Weis, G. D. Fuchs, T. Schenkel, and D. D. Awschalom, "Chip-scale nanofabrication of single spins and spin arrays in diamond," *Nano Lett.* **10**, 3168–3172 (2010).
- ²⁵ P. Spinicelli, A. Dréau, L. Rondin, F. Silva, J. Achard, S. Xavier, S. Bansropun, T. Debuisschert, S. Pezzagna, J. Meijer *et al.*, "Engineered arrays of nitrogen-vacancy color centers in diamond based on implantation of CN⁻ molecules through nanoapertures," *New J. Phys.* **13**, 025014 (2011).
- ²⁶ S. Pezzagna, D. Wildanger, P. Mazarov, A. D. Wieck, Y. Sarov, I. Rangelow, B. Naydenov, F. Jelezko, S. W. Hell, and J. Meijer, "Nanoscale engineering and optical addressing of single spins in diamond," *Small* **6**, 2117–2121 (2010).
- ²⁷ T. Schroder, E. Chen, L. Li, M. Walsh, M. E. Trusheim, I. Bayn, and D. Englund, "Targeted creation and Purcell enhancement of NV centers within photonic crystal cavities in single-crystal diamond," in *CLEO: QELS_Fundamental Science* (Optical Society of America, 2014), pp. FW1B.6.
- ²⁸ T. Schroder, L. Li, E. Chen, M. Walsh, M. E. Trusheim, I. Bayn, J. Zheng, S. Mouradian, H. Bakhru, O. Gaathon *et al.*, "Deterministic high-yield creation of nitrogen vacancy centers in diamond photonic crystal cavities and photonic elements," in *CLEO: QELS_Fundamental Science* (Optical Society of America, 2015), pp. Fth3B-1.
- ²⁹ I. Bayn, E. H. Chen, M. E. Trusheim, L. Li, T. Schröder, O. Gaathon, M. Lu, A. Stein, M. Liu, K. Kisslinger *et al.*, "Generation of ensembles of individually resolvable nitrogen vacancies using nanometer-scale apertures in ultrahigh-aspect ratio planar implantation masks," *Nano Lett.* **15**, 1751–1758 (2015).
- ³⁰ J. F. Ziegler, "SRIM-2003," *Nucl. Instrum. Methods Phys. Res., Sect. B* **219**, 1027–1036 (2004).
- ³¹ B. Hausmann, B. Shields, Q. Quan, Y. Chu, N. De Leon, R. Evans, M. Burek, A. Zibrov, M. Markham, D. Twitchen *et al.*, "Coupling of NV centers to photonic crystal nanobeams in diamond," *Nano Lett.* **13**, 5791–5796 (2013).
- ³² I. Bayn, S. Mouradian, L. Li, J. Goldstein, T. Schröder, J. Zheng, E. Chen, O. Gaathon, M. Lu, A. Stein *et al.*, "Fabrication of triangular nanobeam waveguide networks in bulk diamond using single-crystal silicon hard masks," *Appl. Phys. Lett.* **105**, 211101 (2014).
- ³³ L. Li, I. Bayn, M. Lu, C.-Y. Nam, T. Schröder, A. Stein, N. C. Harris, and D. Englund, "Nanofabrication on unconventional substrates using transferred hard masks," *Sci. Rep.* **5**, 7802 (2015).
- ³⁴ R. A. Gottscho, C. W. Jurgensen, and D. Vitkavage, "Microscopic uniformity in plasma etching," *J. Vac. Sci. Technol., B* **10**, 2133–2147 (1992).
- ³⁵ E. S. Shafqeh and C. W. Jurgensen, "Simulation of reactive ion etching pattern transfer," *J. Appl. Phys.* **66**, 4664–4675 (1989).
- ³⁶ C. Jurgensen, "Sheath collision processes controlling the energy and directionality of surface bombardment in O₂ reactive ion etching," *J. Appl. Phys.* **64**, 590–597 (1988).
- ³⁷ M. J. Burek, N. P. de Leon, B. J. Shields, B. J. Hausmann, Y. Chu, Q. Quan, A. S. Zibrov, H. Park, M. D. Lukin, and M. Loncar, "Free-standing mechanical and photonic nanostructures in single-crystal diamond," *Nano Lett.* **12**, 6084–6089 (2012).

- ³⁸ B. Naydenov, V. Richter, J. Beck, M. Steiner, P. Neumann, G. Balasubramanian, J. Achard, F. Jelezko, J. Wrachtrup, and R. Kalish, "Enhanced generation of single optically active spins in diamond by ion implantation," *Appl. Phys. Lett.* **96**, 163108 (2010).
- ³⁹ S. Pezzagna, B. Naydenov, F. Jelezko, J. Wrachtrup, and J. Meijer, "Creation efficiency of nitrogen-vacancy centres in diamond," *New J. Phys.* **12**, 065017 (2010).
- ⁴⁰ D. Antonov, T. Häußermann, A. Aird, J. Roth, H.-R. Trebin, C. Müller, L. McGuinness, F. Jelezko, T. Yamamoto, J. Isoya *et al.*, "Statistical investigations on nitrogen-vacancy center creation," *Appl. Phys. Lett.* **104**, 012105 (2014).
- ⁴¹ J. Meijer, B. Burchard, M. Domhan, C. Wittmann, T. Gaebel, I. Popa, F. Jelezko, and J. Wrachtrup, "Generation of single color centers by focused nitrogen implantation," *Appl. Phys. Lett.* **87**, 261909 (2005).
- ⁴² C. Kurtsiefer, S. Mayer, P. Zarda, and H. Weinfurter, "Stable solid-state source of single photons," *Phys. Rev. Lett.* **85**, 290 (2000).
- ⁴³ R. Brouri, A. Beveratos, J.-P. Poizat, and P. Grangier, "Photon antibunching in the fluorescence of individual color centers in diamond," *Opt. Lett.* **25**, 1294–1296 (2000).
- ⁴⁴ M. Berthel, O. Mollet, G. Dantelle, T. Gacoin, S. Huant, and A. Drezet, "Photophysics of single nitrogen-vacancy centers in diamond nanocrystals," *Phys. Rev. B* **91**, 035308 (2015).
- ⁴⁵ A. Faraon, P. E. Barclay, C. Santori, K.-M. C. Fu, and R. G. Beausoleil, "Resonant enhancement of the zero-phonon emission from a colour centre in a diamond cavity," *Nat. Photonics* **5**, 301–305 (2011).
- ⁴⁶ J. C. Lee, D. O. Bracher, S. Cui, K. Ohno, C. A. McLellan, X. Zhang, P. Andrich, B. Alemán, K. J. Russell, A. P. Magyar *et al.*, "Deterministic coupling of delta-doped nitrogen vacancy centers to a nanobeam photonic crystal cavity," *Appl. Phys. Lett.* **105**, 261101 (2014).